Theoretical investigation of optical properties and band gap engineering for $Zn_{1-x}TM_xTe$ (TM = Fe, Co) alloys by modified Becke–Johnson potential*

Q Mahmood[1], M Yaseen[2,†], M Hassan[1], Shahid M Ramay[3], and Asif Mahmood[4]

[1] *Materials Growth and Simulation Laboratory, Department of Physics, University of the Punjab, Quaid-i-Azam Campus, 54590, Lahore, Pakistan*
[2] *Department of Physics, University of Agriculture University, Faisalabad 38040, Pakistan*
[3] *Physics and Astronomy Department, College of Science, King Saud University, Riyadh, Saudi Arabia*
[4] *Chemical Engineering Department, College of Engineering, King Saud University, Riyadh, Saudi Arabia*

(Received 1 February 2017; revised manuscript received 1 April 2017; published online 20 June 2017)

The direct band gap ZnTe with transition metal (TM) impurities plays a vital role in optoelectronic and spintronic applications. In the present study, we use the advanced modified Becke–Johnson (mBJ) functional for performing the structural computations and detailed investigations of the optical characters in $Zn_{1-x}TM_xTe$ (TM = Fe, Co) alloys with $0 \leq x \leq 1$. By employing the FP-LAPW method, we determine various optical parameters for the ternary alloys and for the end binaries. The calculated static dielectric constants and optical band gaps for $Zn_{1-x}TM_xTe$ (TM = Fe, Co) have an inverse relation that verifies the Penn model. We find that the static dielectric constant is nearly equal to the square of the static refractive index, and both increase with TM content. Furthermore, we also find a slight shift of peaks to a higher energy region with increasing TM concentration. The decreasing band gap and high value of the absorption in the visible region of electromagnetic spectrum make these alloys suitable for photonic and solar cell applications.

Keywords: amorphous semiconductors, transition metal-doped ZnTe, structural computation, optical property

PACS: 78.66.Jg **DOI:** 10.1088/1674-1056/26/8/087803

1. Introduction

The direct and wide bandgap nature, significant light emitting capabilities exhibited at the working temperature of a device have aroused huge scientific interest for II–VI semiconductors. Therefore, II–VI semiconductors are prospective candidates for various optical devices.[1–4] From this semiconductor family, ZnTe reveals low cost activity in the visible region and the high absorption coefficient illustrating its potential to be employed for the light emitting diodes and the solar cells.[5,6] Moreover, the high quantum efficiency and optimal band gap have made ZnTe an attractive material to replace the silicon based optoelectronic industry.[7] For optical device applications, few experimental reports on ZnTe semiconductors are available in the literature. Furumura *et al.*[8] explored the excitonic effect in the far-ultraviolet region of the absorption spectra measured for ZnTe. Similarly Walter *et al.*[9] calculated the imaginary dielectric constant by using the Kramers–Krong relation from the ZnTe reflectivity spectra. On the other hand, some theoretical works have reported on the ZnTe compound and exploited its potential utilization in optical devices.[9,10]

Recently, diluted magnetic semiconductors (DMSs),[11] in which few cations are replaced with the rare-earth or transition metal magnetic ions have been extensively analyzed. DMSs not only retain their host lattice semiconducting nature but also exhibit magnetic properties induced due to the magnetic dopants. DMSs are considered significant due to the large magnitudes of the Faraday rotation, the g value and the polaronic effect arising from the exchange interactions between the magnetic dopants and the host lattice anions. The lattice constant and the energy band gap can be tuned by adding the magnetic dopant concentration, thus making it possible that the desired properties are exhibited by the DMSs. The low Curie temperature (T_c) and minute spin polarization restrict the practical device applications. Hence, TMs-doped ZnTe alloys depict wide range flexibility over the chemical and physical properties, for example, incorporation of V improves the photorefractive reaction.[12]

The Fe^{2+}-, Co^{2+}-, and Ni^{2+}-doped ZnTe semiconductors have been demonstrated to effectively tune the electronic and optical properties.[13,14] Similarly, Ti-, Cr-, and Mn-doped ZnTe semiconductors result in shifts of the absorption and the reflection spectra due to the dopant nature and the respective concentration.[1] It has been reported that Cr-doped ZnTe reveals maximum absorption in the UV energy range and the band gap decreases compared with the undoped ZnTe.[15,16]

*Project supported by the Deanship of Scientific Research at King Saud University (for Shahid M Ramay) (Grant No. RG 1435-004), the University of the Punjab, Lahore for financial support through Faculty Research Grant Program (for M Hassan), and the HEC Pakistan (Grant No. 21-261/SRGP/R&D/HEC/2014) (for M Yaseen).

†Corresponding author. E-mail: myaseen_taha@yahoo.com

© 2017 Chinese Physical Society and IOP Publishing Ltd

TM-doped ZnTe also finds applications as the back contact for cadmium based solar cells. The Cu-, Mo-, and V-doped ZnTe materials are used for back contact materials but they have a few limitations.[17] For example, doping with Cu increases the electrical conductivity that favors a short circuit current, otherwise this makes a Schottky barrier that could impede the flow of charge carriers.[18] The motivation for changing the non-magnetic ZnTe host lattice to exhibit ferromagnetic properties can be achieved by adding transition metal. Moreover, the attempt to realize ferromagnetism changes the band structures due to the new impurity states that subsequently modify the optical properties. In view of the reported work,[19] the purpose of this article is to perceive the effect of *TM* (Fe and Co) doping of ZnTe on the optical properties through theoretical modeling. To the best of our knowledge, the systematic studies of optical properties of Fe- and Co-doped ZnTe within the full composition range are limited. Consequently, the present study gives magnitudes of some useful optical parameters that can be considered while fabricating various technological important optical devices in future.

2. Method of calculation

The calculations of optical properties for $Zn_{1-x}TM_xTe$ (TM = Fe, Co) with $x = 0.0$–1.0, are performed by employing the FP-LAPW method using the Wien2k code.[20] In the FP-LAPW method, the atomic space is divided into two parts: muffin-tin (MT) and interstitial regions. The solution inside the MT region is of a spherical harmonic type and outside it is of a plane wave type. The density functional theory (DFT)-based Kohn–Sham equations were solved by a self-consistent scheme WC-GGA[21] functional that was used to determine the exchange correlation potential for specifying the total ground state energy. For the band gap improvement and the accurate electronic band structure calculations of semiconductor and insulator materials (spin involved semiconductors, noble gas solids, transition metal-doped alloys, etc.), Becke and Johnson modified the exchange potential (mBJLDA)[22] that has already been used. For estimating the band gap of Fe- and Co-doped ZnTe, we apply this potential to the self-consistent field. The Becke and Johnson modified exchange potential depends on the kinetic-energy density that produces the exact shape of the band structure.

The bulk ZnTe with experimental lattice constant 6.089 Å[23] in the zinc blende phase has space group $F43m$ (No. 216) with atomic positions Zn (0 0 0) and Te (1/4 1/4 1/4). The cases of substitution of *TM* into ZnTe at $x = 0.125$, 0.50 generate tetragonal distortions with space groups: $P\text{-}4m2$ and $P\text{-}42m$, respectively, whereas at $x = 0.25$, 0.75, only the cubic structure (space group: $P43m$) is stabilized. The relativistic Dirac equation is solved for core and valence states of Zn, Fe, Co, and Te by using scalar relativistic estimations. The energy separation is taken to be -6 Ry (1 Ry = 13.6056923 eV). To converge the eigenvalue, the matrix size is controlled by the product $R_{\mathrm{MT}} \times K_{\max} = 8$, where R_{MT} shows the least muffin-tin radius while $K_{\max}$ represents the reciprocal lattice vector. The individual values of R_{MT} for Fe and Co are taken to be 2.1 a.u. and 1.95 a.u. respectively. The maximum value of the angular momentum vector is kept at 10 and Fourier expansion vector $G_{\max} = 16$ (Ry)$^{1/2}$. Furthermore, the k-mesh selected is $10 \times 10 \times 10$ and total energy convergence is less than 10^{-4} Ry.

The optical properties for $Zn_{1-x}TM_xTe$ (TM = Fe, Co) are mostly studied in terms of dielectric function $\varepsilon(\omega) = \varepsilon_1(\omega) + i\varepsilon_2(\omega)$ that has real $\varepsilon_1(\omega)$ and imaginary $\varepsilon_2(\omega)$ dielectric parts. The dielectric tensor is extracted from the computed band structures by employing the joint density of states and the transition matrix elements. Only the direct inter-band contributions are considered. Cottenier[24] and Ehrenreich and Cohen[25] briefly described $\varepsilon_2(\omega)$ in terms of the following equation:

$$\varepsilon_2(\omega) = \frac{e^2 h'}{\pi m^2 \omega^2} \sum_{v,C} \int_{BZ} |M_{Cv}(k)|^2 \, \delta[\omega_{Cv}(k) - \omega] \, \mathrm{d}^3 k, \quad (1)$$

where the volume integral of the dipole matrix is confined up to the first Brillion zone and $M_{Cv}(k) = \langle u_{Ck} | e\nabla | u_{vk} \rangle$ gives the evidence about the inter-band transitions. The equation $\omega_{Cv}(k) = E_{Ck} - E_{vk}$ reveals the energy involved during the electron transitions from valence to conduction states and represents the polarization vector of the electric field. The real dielectric function $\varepsilon_1(\omega)$ is computed from the imaginary part by using Kramers–Kronige expressions:[26]

$$\varepsilon_1(\omega) = 1 + \frac{2}{\pi} P \int_0^{\infty} \frac{\omega' \varepsilon_2(\omega')}{\omega'^2 - \omega^2} \, \mathrm{d}\omega'. \quad (2)$$

From real and imaginary dielectric functions, we can calculate the refractive index $n(\omega)$ and the extension coefficient $k(\omega)$ by using the following relations:

$$n(\omega) = \left[\frac{\varepsilon_1(\omega)}{2} - \frac{\sqrt{\varepsilon_1^2(\omega) + \varepsilon_2^2(\omega)}}{2} \right]^{1/2} \quad (3)$$

and

$$k(\omega) = \left[\frac{-\varepsilon_1(\omega)}{2} + \frac{\sqrt{\varepsilon_1^2(\omega) + \varepsilon_2^2(\omega)}}{2} \right]^{1/2}. \quad (4)$$

Reflectivity for normal incidence of light is the ratio of the reflected to the incident photon energy and is calculated from the following relation:

$$R = \frac{(n-1)^2 + k^2}{(n+1)^2 + k^2}. \quad (5)$$

The absorption coefficient describes the percentage attenuation incident intensity when light propagates through unit distance in a material. It is a replica of extension coefficient $k(\omega)$ and is given below

$$\alpha(\omega) = 4\pi k(\omega)/\lambda, \quad (6)$$

where λ is the wavelength of the incident energy. Another important parameter that gives energy loss per unit distance when an electron moves in the material is represented as $L(\omega)$ and can be computed from

$$L(\omega) = \mathrm{Im}\left(-1/\tilde{\varepsilon}(\omega)\right). \tag{7}$$

The optical conductivity $\sigma(\omega)$ is presented by the following expression:

$$\sigma(\omega) = \left(2W_{Cv}h'\omega\right)/E_0, \tag{8}$$

where W_{Cv} represents the transition mobility per unit time.

3. Results and discussion

In our previous work, we have already optimized the present structures in paramagnetic, antiferromagnetic and ferromagnetic phases, respectively, and have confirmed the stable ferromagnetic phase due to relatively how much energy is released. Moreover, the formation of negative enthalpy ensures ferromagnetic phase stability.[19] The optical properties play a vital role in examining the internal structure of any material. Particularly in optoelectronics, the optical properties of a material reveal its suitability for technological applications. In the present work, we demonstrate the computed optical properties for $Zn_{1-x}TM_xTe$ (TM = Fe, Co). The refractive index and band gap perform a crucial role in selecting the DMS for optoelectronic devices. Therefore, both parameters significantly affect the material choice for various applications. Our previous report[19] showed that Fe and Co doping causes a direct band gap for the up spin channel, and the down spin channel, illustrating a considerable exchange splitting. However, Fe and Co impurity states also operate within the computed band structures. The absorption threshold for the impinging photons is related to the band gap, while the refractive index reveals material transparency in a specific incident energy range. The dielectric constant is the elementary property of the material and directly related to the value of the refractive index, and can be determined by using various methods. Similarly, various optical properties can be illustrated by different computed optical parameters.

Figures 1(a)–1(f) show the geometrical structures of $Zn_{1-x}TM_xTe$ (TM = Fe and Co) with $x = 0.0$, 0.125, 0.25, 0.50, 0.75, and 1.0, respectively. The structural symmetry is very important for describing the optical response of a material. Figures 1(a)–1(f) clearly show that the structural symmetry is lowest at $x = 0.50$ and highest at $x = 0.75$. Therefore, variation of structural symmetry changes the properties of the alloys abruptly at high concentrations as can be seen in Table 1.

Moreover, the static dielectric constant and optical band gap find an inverse variation, as shown in Fig. 2. This inverse relation can be justified in terms of Penn's model, which is mathematically expressed as[27,28]

$$\varepsilon_1(0) \approx 1 + (\hbar\omega_p/E_g)^2. \tag{9}$$

Here ω_p, E_g, and $\hbar$ show the plasma frequency, the band gap, and the Planck constant, respectively. The relation given by Penn's model can be used to extract the band gap when the remaining parameters are known. The computed static dielectric constant $\varepsilon_1(0)$ and optical band gap for $Zn_{1-x}TM_xTe$ with $x = 0.0$, 0.125, 0.25, 0.50, 0.75, and 1.0 are presented in Table 1.

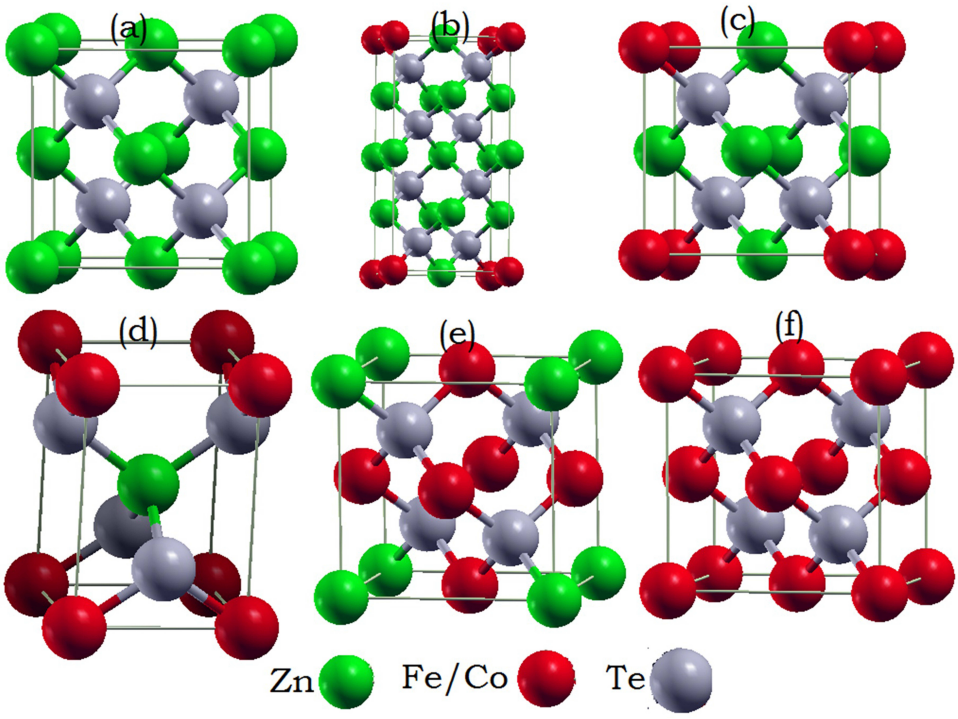


Fig. 1. (color online) Geometrical structures for $Zn_{1-x}TM_xTe$ (TM = Fe, Co) alloys at x = (a) 0.0, (b) 0.125, (c) 0.25, (d) 0.50, (e) 0.75, and (f) 1.0. The red, green, and gray balls represent the Fe/Co, Zn, and Te atoms respectively.

Table 1. Calculated optical parameters for $Zn_{1-x}TM_xTe$ (TM = Fe, Co) alloys at $x = 0.0$–1.0 by using mBJ potential.

X	E_g^d/eV	$\varepsilon_1(0)$	$R(0)$	$n(0)$	Critical points values			
					ε_2	K	A	σ
ZnTe	2.39	6.70	0.196	2.58	2.52	2.63	2.71	3.11
Exp.	2.39[a]	7.3[b]		2.40[c]	2.30[c]		2.72[c]	
$Zn_xFe_{1-x}Te$								
0.125	2.31	7.12	0.202	2.70	2.21	2.40	2.48	2.33
0.25	2.25	7.52	0.220	2.80	2.12	2.06	2.31	2.06
0.50	2.10	7.73	0.226	2.85	2.06	1.97	2.20	1.99
0.75	2.05	14.13	0.338	3.76	0.15	0.09	0.77	1.50
1.0	1.80	58.61	0.597	7.70	0.05	0.02	0.28	0.20
$Zn_xCo_{1-x}Te$								
0.125	2.35	6.26	0.184	2.50	2.02	2.39	2.54	2.95
0.25	2.25	7.12	0.206	2.66	1.74	2.06	2.25	2.44
0.50	2.19	7.52	0.216	2.76	1.42	1.87	1.97	2.14
0.75	2.10	14.18	0.229	2.83	0.68	0.62	0.87	1.89
1.0	2.00	15.51	0.355	3.94	0.11	0.13	0.32	0.15

[a]Ref. [39], [b]Ref. [40], [c]Ref. [41].

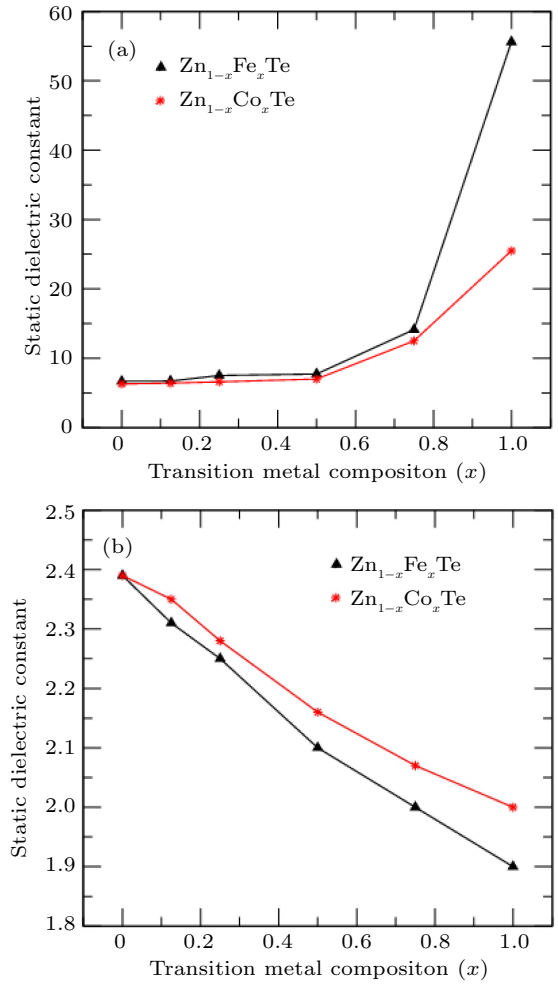


Fig. 2. (color online) Plots of calculated static dielectric constant and optical band gap versus transition metal composition for both $Zn_{1-x}Fe_xTe$ and $Zn_{1-x}Co_xTe$ with $x = 0.0$–1.0.

The wide spectrum of optical properties is usually explained in terms $\varepsilon(\omega)$, $n(\omega)$, and $k(\omega)$. The dielectric constant comprehensively shows a material behavior against the incident electric field. The real and imaginary dielectric functions for $Zn_{1-x}TM_xTe$ (TM = Fe and Co) alloys are plotted in Figs. 3 and 4. The real dielectric constant $\varepsilon_1(\omega)$ reveals a material's polarization. It can be observed in Figs. 3(a) and 4(a) that the real dielectric constant starts to increase from its zero frequency value (as shown in Table 1) and reaches peak values 3.56 eV, 3.58 eV, 3.64 eV, 4.21 eV, 2.27 eV, and 2.84 eV for $x_{Fe} = 0.0$, 0.125, 0.25, 0.50, 0.75, and 1.0, respectively and 3.58 eV, 3.78 eV, 3.88 eV, 2.27 eV, 4.09 eV, and 2.35 eV for $x_{Co} = 0.0$, 0.125, 0.25, 0.50, 0.75, and 1.0, respectively. After reaching peak values, the real part of the dielectric constant starts to decrease and becomes zero at 5.31 eV, 5.67 eV, 5.89 eV, 6.07 eV, 6.87 eV, and 7.53 eV for $x_{Fe} = 0.0$, 0.125, 0.25, 0.50, 0.75, and 1.0, respectively. A similar trend for Co concentrations is observed. It becomes zero at 5.27 eV, 6.01 eV, 6.05 eV, 6.18 eV, 6.67 eV, and 8.17 eV. For further increasing the value of energy the real part of the dielectric becomes negative up to 13 eV for both Fe and Co concentrations and again becomes zero. The negative $\varepsilon_1(\omega)$ in a particular region of energy represents the medium which totally reflects incident radiation to show a metallic character.[29] The graphs also shows that the behaviors of these compounds are linear for small doping of Fe and Co and at high composition their behaviors are different, specifically at $x = 0.75$, which is due to the variations in structural symmetry. The structure has the lowest and highest symmetries at $x = 0.50$ and $x = 0.75$, respectively. For end binaries FeTe and CoTe, the static parts of their real dielectric constants are totally different. These compounds have initially a large value of the dielectric constant, which drastically drops to the negative value in the low energy region and then follows a similar trend for both dopants.

The imaginary dielectric constant, $\varepsilon_2(\omega)$ plays a very important role in studying the optical properties, therefore, their computed values are plotted in Figs. 3(b) and 4(b), where it is evident that the effective energy range for absorption increases, while the peak height decreases due to Fe and Co doping into ZnTe. It is clear that the absorption starts at a low value of energy and reaches peak values of 5.08 eV, 5.10 eV, 5.12 eV, 5.14 eV, 5.10 eV, and 5.25 eV, due to Fe doping, and 5.09 eV, 5.28 eV, 5.38 eV, 5.54 eV, 5.10 eV, and 5.23 eV, due to codoping with $x = 0.0$, 0.125, 0.25, 0.50, 0.75, and 1.0, respectively. It can also be observed that at low Fe and Co content, there appear absorption peaks that slightly shift towards higher energy, however, at high doping content (at $x = 0.50$ to 1.0), the $\varepsilon_2(\omega)$ first decreases and then again increases, which is due to the variation of structural symmetry. After reaching a peak value it starts to decrease monotonically and becomes constant after 13 eV. The peaks appear due to the direct electronic transitions from the occupied state (valence) to the unoccupied (conduction) state.[30] Figures 3(b) and 4(b) also show that almost strong absorption is exhibited by all $Zn_{1-x}TM_xTe$ compounds within 2 eV–14 eV. This energy region contains different peaks arising from the inter-band electronic transitions.

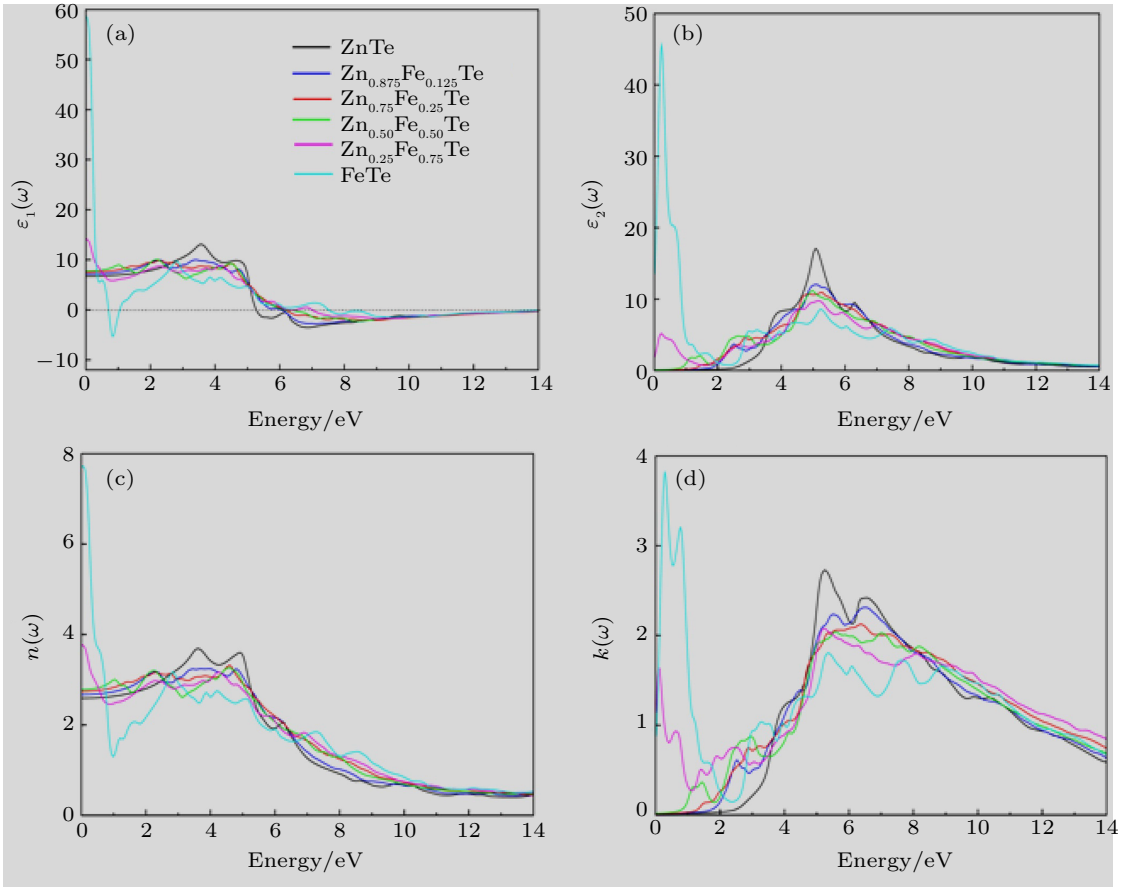


Fig. 3. (color online) Plots of calculated (a) real $\varepsilon_1(\omega)$, and (b) imaginary $\varepsilon_2(\omega)$ dielectric constant, (c) refractive index $n(\omega)$, (d) extinction coefficient $k(\omega)$ versus energy for $Zn_{1-x}Fe_xTe$ alloys with $x = 0.0$–1.0.

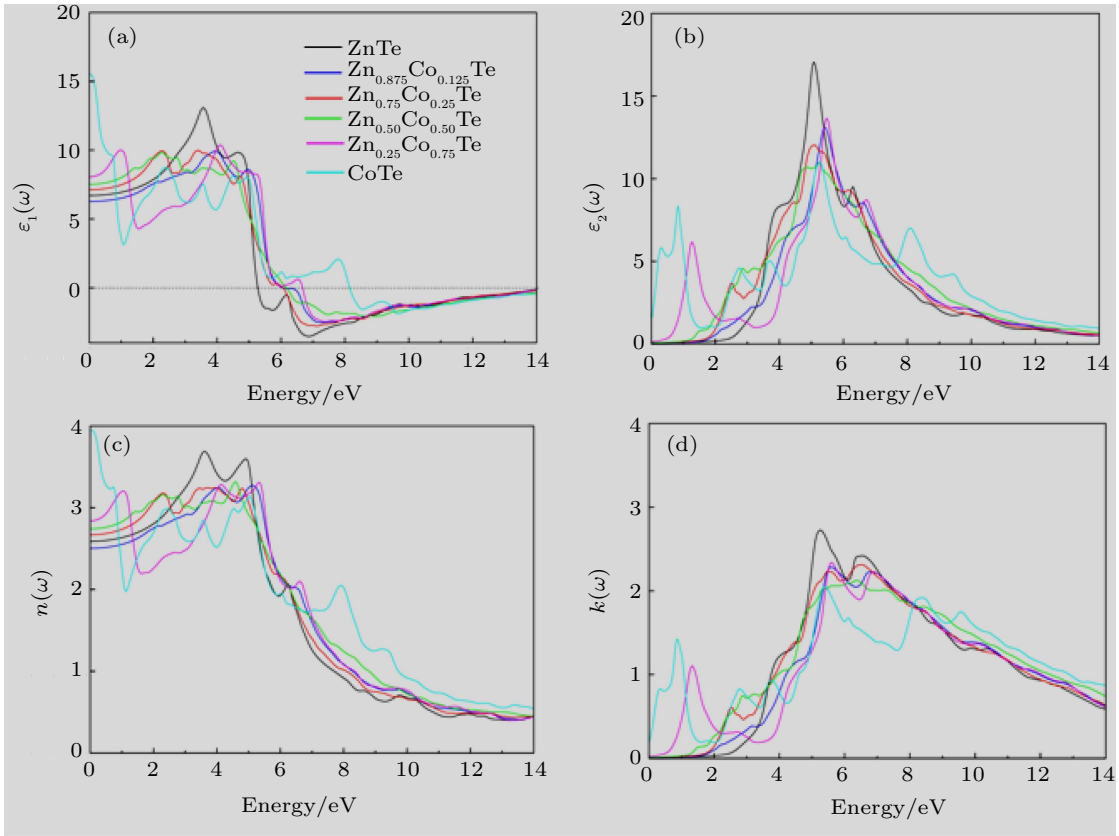


Fig. 4. (color online) Plots of computed (a) real $\varepsilon_1(\omega)$ and (b) imaginary $\varepsilon_2(\omega)$ dielectric constant, (c) refractive index, $n(\omega)$, (d) extinction coefficient $k(\omega)$ versus energy for $Zn_{1-x}Co_xTe$ with $x = 0.0$–1.0.

The optical behaviors elucidated by real and imaginary dielectric functions can also be described by refractive index $n(\omega)$ and the extinction coefficient $k(\omega)$, respectively, of $Zn_{1-x}TM_xTe$ alloys, which can be calculated from the equations $n^2 - k^2 = \varepsilon_1(\omega)$ and $2nk = \varepsilon_2$. The calculated values of refractive index $n(\omega)$ and extinction coefficient $k(\omega)$ for $Zn_{1-x}TM_xTe$ alloys at $x = 0.0$, 0.125, 0.25, 0.50, 0.75, and 1.0 are shown in Figs. 3(c), 3(d), 4(c), and 4(d), respectively. An $n(\omega)$ spectrum is spread over a large energy range for each of the studied compounds. The computed refractive index $n(\omega)$ exhibits a direct relation to the dielectric constant $\varepsilon(\omega)$.[31] From the above equations, it is evident that the behaviors of $\varepsilon_1(\omega)$ and $\varepsilon_2(\omega)$ are nearly similar to $n(\omega)$ and $k(\omega)$, respectively. Smaller $k(\omega)$ illustrates that the total density of atomic states contributes little to the absorption phenomenon.

Moreover, the inverse relation between the critical values of $n(0)$ and $k(0)$ is also evident as shown in Table 1. The $n(0)$ increases with TM concentration, which could be employed to tune the band gap for a specific electronic device (band gap decreases with increasing refractive index). It can also be seen from Table 1 that the values of $n(0)$ for $Zn_{1-x}TM_xTe$ alloys increase with x. Moreover, the computed values also satisfy the formula $n_0^2 = \varepsilon_1(0)$ which illustrates the accuracies of these computations. On the other hand, the peak values of refractive index $n(\omega)$ shift towards higher energy and peak intensities decrease with the Fe and Co content in the ZnTe host lattice. From Figs. 3(c) and 4(c), a hump appearing in the middle of the graph vanishes at higher energy. This could be attributed to the fact that beyond a certain incident energy the transparency decreases, therefore, the absorption of the impinging energy improves.[32]

The values of extinction coefficient $k(\omega)$ calculated for $Zn_{1-x}TM_xTe$ (TM = Fe and Co) alloys with $x = 0.0$–1.0, are shown in Figs. 3(d) and 4(d). The $k(\omega)$ provides information about the absorption of light and the optical behaviors of a material at the band edge. The frequency dependent $k(\omega)$ increases monotonically in the visible region and has a peak value in near the UV-region showing maximum absorption. The $k(\omega)$ has almost the same characteristic as imaginary dielectric constant $\varepsilon_2(\omega)$.[33,34] The peaks in $k(\omega)$ and $\varepsilon_2(\omega)$ are due to the inter-band electronic transitions.

To understand the surface behavior of the material, its reflectivity (ratio of incident light intensity to reflected light intensity) is also computed. Figures 5(a) and 6(a) show the plots of calculated reflectivity versus energy for $Zn_{1-x}TM_xTe$ (TM = Fe and Co) with $x = 0.0$–1.0. It is evident in Table 1 that the zerofrequency value of reflectivity increases with dopant concentration increasing. Furthermore, it could also be seen in Figs. 5(a) and 6(a) that reflections are enhanced as the peak value of incident energy increases in sequence: 5.25 eV, 5.50 eV, 6.37 eV, 7.11 eV, 5.29 eV, and 5.31 eV for Fe and 5.25 eV, 5.46 eV, 5.55 eV, 5.57 eV, 5.33 eV, and 5.36 eV for Co, with $x = 0.0$, 0.125, 0.25, 0.50, 0.75 and 1.0, respectively. These peaks are constituted due to the least absorptive nature shown by the studied compounds in the specific energy ranges. In addition, the reflectivity spectrum appears within 2 eV–14 eV and collective plasma resonance occurs above this energy. The plasma resonance effect can be measured from $\varepsilon_2(\omega)$. The reflectivity plots depict an interesting behavior because the increasing of dopant induces a shift towards higher energy, which is consistent with the trend observed for $\varepsilon_2(\omega)$.[28,35]

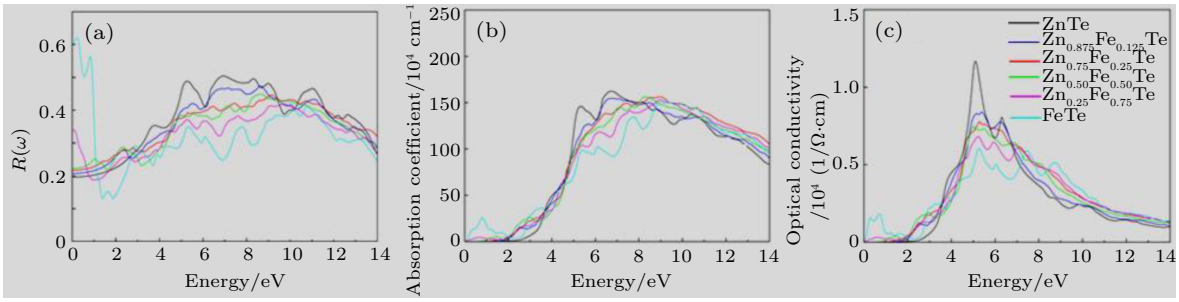


Fig. 5. (color online) Plots of (a) reflectivity (R), (b) absorption coefficient (α), and (c) optical conductivity (σ) versus energy for $Zn_{1-x}Fe_xTe$ with $x = 0.0$–1.0.

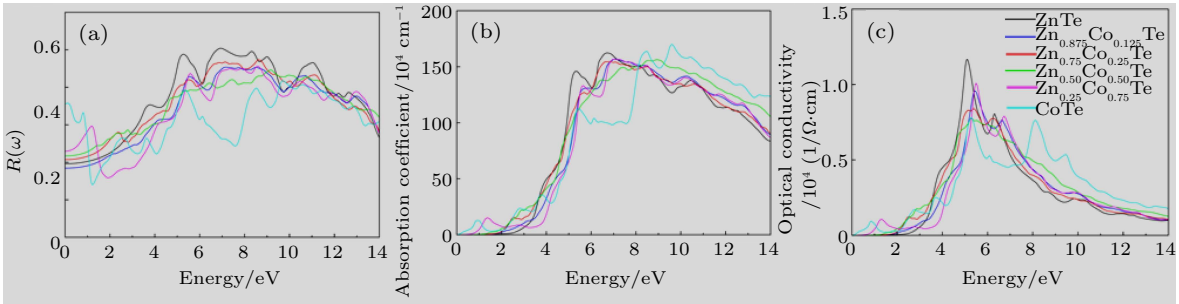


Fig. 6. (color online) Variations of calculated (a) reflectivity (R), (b) absorption coefficient (α), and (c) optical conductivity (σ) with energy for $Zn_{1-x}Co_xTe$ with $x = 0.0$–1.0.

The energy absorption appears at a resonant atomic transition frequency and reveals the decay mechanism of incident light propagating through the lattice. The absorption coefficients for $Zn_{1-x}TM_xTe$ (TM = Fe, Co) alloys calculated ina wide energy range (from infrared region to ultraviolet region 0 eV–14 eV) are shown in Figs. 5(b) and 6(b). In the low energy region there is no absorption, while absorptions start from 2 eV and approach to maximum values 6.67 eV, 6.68 eV, 7.39 eV, 7.40 eV, 8.93 eV, and 8.97 eV due to Fe doping and 6.67 eV, 6.68 eV, 6.98 eV, 7.43 eV, 6.96 eV, and 8.51 eV, due to Co doping into ZnTe with $x = 0.0$, 0.125, 0.25, 0.50, 0.75, and 1.0, respectively, and decrease at even higher energies and finally attain their corresponding constant levels. The studied compounds are nearly transparent to the infrared light, and start the absorption in the visible region, then reach to their corresponding maximum values in the mid ultraviolet region. Therefore, TM doping plays a major role in tuning the exhibited absorption in the visible region. Pure ZnTe shows distinct and sharp absorption peaks. The TM doping suppresses the absorption peaks and widens the absorption spectrum that looks extended at lower energies illustrating a band gap reduction in $Zn_{1-x}TM_xTe$ due to dopant concentrations. For example, pure ZnTe has a band gap of 2.39 eV, which reduces to 2.0 eV and 1.80 eV for the end binaries FeTe and CoTe respectively. The experimental band gap for pure ZnTe is 2.26 eV and CoTe is 2.05 eV, confirming the accuracy of our theoretical results.[36–38] The Fe doping and Co doping induced red shift in the absorption band could be explained by the presence of p–d exchange resulting from the interactions of the conduction electrons with the localized d electrons of TM. The decreasing of band gap with doping of TM increasing may be attributed to the various band states moving more closer, which occurs due to the incorporation of impurity-induced states inside the band gap and around the Fermi level. Furthermore, the critical values of absorption show the decreasing trend with increasing TM composition (see Table 1), confirming that less energy is required for the electrons to jump from the valence to the conduction band at resonance frequency. In fact, these peaks represent the strong absorptions of energy which offers the new functionality in materials for specific applications.

The calculated optical conductivity $\sigma(\omega)$ spectra for $Zn_{1-x}TM_xTe$ alloys at $x = 0.0$, 0.125, 0.25, 0.50, 0.75, and 1.0 are depicted in Figs. 5(c) and 6(c), which start to increase in the low energy region (nearly 2 eV) and become maxima at 5.10 eV, 5.17 eV, 5.33 eV, 5.48 eV, 5.23 eV, and 5.25 eV when Fe is employed as dopant and 5.14 eV, 5.18 eV, 5.30 eV, 5.40 eV, 5.25 eV, and 5.32 eV, when Co dopants are used in ZnTe with $x = 0.0$, 0.125, 0.25, 0.50, 0.75, and 1.0, respectively. After attaining maxima, they decease and become constant around $x = 14$ eV. The peak values are shifted towards high energy for a dopant concentration less than 0.50, and decrease at $x = 0.50$, while they again increase at $x = 0.75$, which is due to the structural symmetry modifications. The energy losses by the electrons moving through the $Zn_{1-x}TM_xTe$ alloys are also computed and presented in Figs. 7(a) and 7(b). The energy losses maintain minima up to 5 eV and then start to increase and attain the values within 15 eV–20 eV, however, at even higher energies they continue to decrease till 35 eV. Moreover, the peaks are shifted to higher energy with enhancing the dopant (Fe and Co) content into the ZnTe host lattice. The peak values in the specific energy range are related to the plasma frequency.

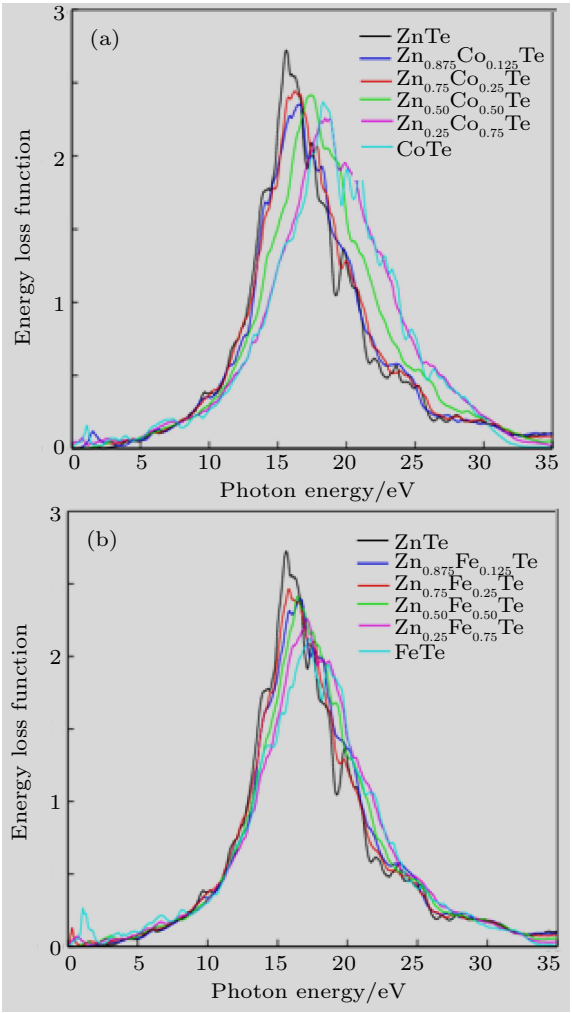


Fig. 7. (color online) Plots of energy loss function versus photon energy for $Zn_{1-x}Co_xTe$ and $Zn_{1-x}Fe_xTe$ with $x = 0.0$–1.0.

The studied compounds can be considered to have low and high dopant content end binaries (FeTe, CoTe, etc.). A compound with a low dopant concentration results in a linear variation in the optical property due to the stable symmetric ZB phase, while a high dopant concentration ($x = 0.75$) results in quite an abrupt variation in the exhibited property. Such a response occurs due to the structural symmetry change resulting from the dopant in the studied compound, which is minimum at $x = 0.50$ and maximum at $x = 0.75$. Some extra peaks in the low energy region also occur due to Fe and Co doping, which reveals that the studied compounds could also respond to these specific energies suggesting useful device applications.

Furthermore, the incident electromagnetic energy can be divided into three regions: infrared (IR), visible, and ultraviolet (UV). The negligible absorption occurs in the infrared region, while within the visible region (1.9 eV to 3.1 eV) absorption starts and attains a maximum in the ultraviolet region. The behaviors at 50% and 75% doping of Fe and Co are quite different from those of the other compounds because of strong hybridizations between Fe-3d and Te-2p states and between Co-3d and Te-2p states. Moreover, all the computed optical parameters reveal considerable variations in the visible and the ultraviolet regions, where minimum optical losses occur, which makes them suitable for optoelectronic devices. In addition, the hybridization process causes a stable ferromagnetic state that affects the band structure, and hence, the introduction of magnetic characteristics offers opportunities to tune the optical parameters exhibited by the host lattice, which suggests the potential optical device applications of the studied compounds.

4. Conclusions

The optical properties calculated for 0 eV–14 eV are strongly dependent on the TM concentration. The static refractive index $n(0)$, reflectivity $R(0)$, and dielectric constant $\varepsilon_1(0)$ increase with dopant concentration in $Zn_{1-x}TM_xTe$ (TM = Fe, Co and x = 0.0–1.0). The negative values of the real dielectric constant appearing within low energy reveal the total reflection for the incident radiations; therefore, metallic behavior is demonstrated. The maximum absorption in the visible region suggests that the studied materials are suitable for photonic and solar cell applications. The reflectivity peaks shift towards higher energy due to TM doping, which is consistent with the observations about imaginary dielectric constant. The band gap tuning could be realized from 2.39 eV to 2.0 eV for un-doped ZnTe and 1.80 eV for $Zn_{1-x}TM_xTe$ with TM = Fe, Co, respectively, in the visible region, indicating potential applications of the studied compounds in various optical devices, like solar cells, LEDs, etc.

References

[1] Zaari H, Boujnah M, El Hachimi A, Benyoussef A and El Kenz A 2014 *Opt. Quantum Electron.* **46** 75
[2] Aqili A K, Ali Z and Maqsood A 2000 *Appl. Surf. Sci.* **67** 1
[3] Ibrahim A, El-Sayed N, Kaid M andAshour A 2004 *Vacuum* **75** 189
[4] Dean P J 1979 *Luminescence* **18** 19
[5] TanakaT, MatsunoY J, KumeY, Nishio M, Guo Q X and Ogawa H 2004 *Phys. Status Solidi* **1** 1026
[6] Bozzini B, Baker M A, Cavallotti P L, Cerri E and Lenardi C 2000 *Thin Solid Films* **388** 361
[7] Rao G K, Bangera K V and Shiva Kumar G K 2010 *Mater. Res. Bull.* **45** 1357
[8] Furumura Y, Ebina A and Takahashi T 1979 *Phys. Rev. B* **19** 1031
[9] Walter J P, Cohen M L, Ṕetroff Y and Balkanski M 1970 *Phys. Rev. B* **1** 2661
[10] Karazhanov S Z, Ravindran P, Kjekshus A, Fjellvåg H and Svensson B G 2007 *Phys. Rev. B* **75** 155104
[11] Furdyna J K 1998 *J. Appl. Phys.* **64** R29
[12] Kreissl J and Irmscher K 1996 *Phys. Rev. B* **53** 1917
[13] Ummartyotin S, Bunnak N, Juntaro J, Sain M and Manuspiya H 2012 *Solid State Sci.* **14** 3
[14] Monika Mall and Lokendra Kumar 2010 *J. Lumin.* **130** 4
[15] Dinesh Sharma C, Subodh Srivastava, VijayY K and SharmaY K 2013 *Adv. Mater. Lett.* **4** 68
[16] Bose D N and Bhunia S 2005 *Bull. Mater. Sci.* **28** 647
[17] Akram Aqili K S, Ahmad Saleh J, Zulfiqar Ali and Al-OmariS 2012 *J. Alloys. Compd.* **520** 83
[18] Gessert T A 1995 *J. Electron. Mater.* **24** 1443
[19] Mahmood Q, Javed A, Murtaza G and Alay-e-Abbas S M 2015 *Mater. Chem. Phys.* **162** 831
[20] Blaha P, Schwarz K, Madsen G K H, Kvasnicka D and Luitz J 2001 WIEN2K, LAPW+lo, Karl Heinz Schwarz, Techn. Universität, Vienna Austria
[21] Wu Z and Cohen R E 2006 *Phys. Rev. B* **73** 235116
[22] Tran F and Blaha P 2009 *Phys. Rev. Lett.* **102** 226401
[23] Madelung O, Schulz M and Weiss H 1982 *Springer Berlin* **17**
[24] S Cottenier, 2002 *Density Functional Theory and the family of (L) APW Methods Step by Step: Introduction* pp. 35–39
[25] Ehrenreich H and Cohen M L 1959 *Phys. Rev.* **115** 786
[26] Huang Y H, Jie W Q and Zha G Q 2013 *J. Alloys. Compd.* **555** 117
[27] Penn D 1962 *Phys. Rev.* **128** 2093
[28] Noor N A, Ikram N, Ali S, Nazir S, Alay-e-Abbas S M and Shaukat A 2010 *J. Alloys Compd.* **507** 356
[29] Xu B, Li X, Sun J and Yi L 2008 *Eur. Phys. J. B* **66** 483
[30] Hayatullah, Murtaza G, Khenata R, Mohammad S, Naeem S, Khalid M N and Manzar A 2013 *Physica B* **420** 15
[31] Amin B, Ahmad I, Maqbool M, Goumri-Said S and Ahmad R 2011 *J. Appl. Phys.* **109** 023109
[32] Nazir G, Ahmad A, Khan M and Tariq S 2015 *Comp. Conden. Mater.* **4** 32
[33] Wang L J, Kuzmich A and Dogariu A 2000 *Nature* **406** 277
[34] Mognai D, Ranfagni A and Ruggeri R 2000 *Phys. Rev. Lett.* **84** 4830
[35] Reshak A H, Charifi Z and Baaziz H 2007 *Eur. Phys. J. B* **60** 463
[36] Khan M S, Ashiq M N, Ehsan M F, He T and Ijaz S 2014 *Appl. Catalysis A* **S0926-860X** 567
[37] Ying O C, Hua X Z, Zhen O Q, Dong L, Qing Y and Sheng L M 2007 *Chin. Phys.* **15** 1585
[38] Hannachi L and Bouarissa N 2009 *Physica B* **404** 3650
[39] Lempert R G, Hass K C and Ehrenreich H 1987 *Phys. Rev. B* **36** 1111
[40] Kootstra F, de Boeij P L and Snijders J C 2000 *Phys. Rev. B* **62** 7071
[41] Zaari H, Boujnah M, El Hachimi A, Benyoussef A and El Kenz A 2014 *Opt. Quantum Electron.* **46** 75